■ **Metalloradicals**

Metalloradical Cations and Dications Based on Divinyldiphosphene and Divinyldiarsene Ligands

Mahendra K. Sharma,[a] Dennis Rottschäfer,[a] Beate Neumann,[a] Hans-Georg Stammler,[a] Sergi Danés,[b] Diego M. Andrada,*[b] Maurice van Gastel,[c] Alexander Hinz,[d] and Rajendra S. Ghadwal*[a]

Abstract: Metalloradicals are key species in synthesis, catalysis, and bioinorganic chemistry. Herein, two iron radical cation complexes (**3-E**)GaCl$_4$ [(**3-E**)$^{\bullet+}$ = [{(IPr)-C(Ph)E}$_2$Fe(CO)$_3$]$^{\bullet+}$, E = P or As; IPr = C{(NDipp)CH}$_2$, Dipp = 2,6-iPr$_2$C$_6$H$_3$] are reported as crystalline solids. Treatment of the divinyldipnictenes {(IPr)C(Ph)E}$_2$ (**1-E**) with Fe$_2$(CO)$_9$ affords [{(IPr)C(Ph)E}$_2$Fe(CO)$_3$] (**2-E**), in which **1-E** binds to the Fe atom in an allylic (η^3-EEC$_{vinyl}$) fashion and functions as a 4e donor ligand. Complexes **2-E** undergo 1e oxidation with GaCl$_3$ to yield (**3-E**)GaCl$_4$. Spin density analysis revealed that the unpaired electron in (**3-E**)$^{\bullet+}$ is mainly located on the Fe (52–64%) and vinylic C (30–36%) atoms. Further 1e oxidation of (**3-E**)GaCl$_4$ leads to unprecedented η^3-EEC$_{vinyl}$ to η^3-EC$_{vinyl}$C$_{Ph}$ coordination shuttling to form the dications (**4-E**)(GaCl$_4$)$_2$.

Introduction

The isolation and exploration of stable radicals is an area of high current interest because of their intriguing electronic structures and properties;[1] hence, they offer promising perspectives in synthesis, catalysis,[2] and materials science.[3] Metalloradicals based on earth-abundant 3d metals,[4] which preferably undergo single-electron transfer reactions and frequent-

ly involve open-shell intermediates,[5] are of particular interest in organometallic chemistry[6] and sustainable synthesis.[7] The use of geometrically constrained alkene-containing ligands, bulky porphyrins in particular,[8] is a remarkably successful approach to stabilizing mononuclear metalloradicals.[9]

Diphosphenes **II**,[10] the phosphorus analogues of ubiquitous alkenes **I** (Figure 1), are an interesting class of functional molecules as they, in addition to the P=P bond, feature a lone pair of electrons on the phosphorus atom.[11] Therefore, **II** may, in principle, serve as σ and π donors. However, the HOMO of **II** is invariably the lone pair at the phosphorus atom, while the P=P π-bonding orbital is very low lying, and thus usually inaccessible for chemical bonding.[10, 12] Unlike alkenes **I**, diphosphenes **II** are highly reactive and their isolation requires the use of bulky substituents at the phosphorus atoms.[13] Over the years, a variety of metal complexes derived from stable diphosphenes and heavier congeners have been reported.[13–14] Interestingly, there is only one example of a stable diphosphene metalloradical cation (**III**) known to date, while analogous heavier pnictogen derivatives have remained virtually unknown.[15] The scarcity of stable diphosphene radical cations and anions is most likely because of the large HOMO–LUMO

[a] Dr. M. K. Sharma, Dr. D. Rottschäfer, B. Neumann, Dr. H.-G. Stammler, Priv.-Doz. Dr. R. S. Ghadwal
Molecular Inorganic Chemistry and Catalysis
Inorganic and Structural Chemistry, Center for Molecular Materials
Faculty of Chemistry, Universität Bielefeld
Universitätsstrasse 25, 33615, Bielefeld (Germany)
E-mail: rghadwal@uni-bielefeld.de
Homepage: www.ghadwalgroup.de

[b] S. Danés, Dr. D. M. Andrada
Allgemeine und Anorganische Chemie
Universität des Saarlandes, Campus C4.1, 66123 Saarbrücken (Germany)
E-mail: diego.andrada@uni-saarland.de

[c] Dr. M. van Gastel
Max-Planck-Institut für Kohlenforschung Molecular Theory and Spectroscopy, Kaiser-Wilhelm-Platz 1, Mülheim an der Ruhr 45470 (Germany)

[d] Dr. A. Hinz
Institute of Inorganic Chemistry, Karlsruhe Institute of Technology (KIT)
Engesserstrasse 15, 76131 Karlsruhe (Germany)
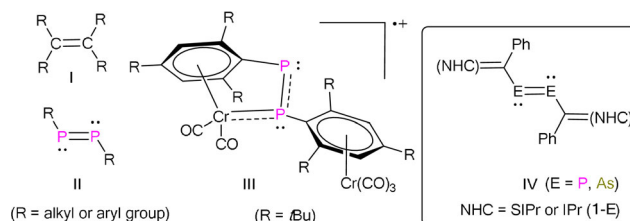
Figure 1. Schematic representation of **I–IV**.

Chemistry–A European Journal

Full Paper
doi.org/10.1002/chem.202100213

Chemistry
Europe
European Chemical
Societies Publishing

energy gap.[10,12,16] The lowering of the HOMO–LUMO energy gap by π conjugation is fundamental to organic chemistry and materials science.[17] Recently, we reported stable dipnictenes **IV**[18] as well as pnictinidene complexes[19] containing N-heterocyclic vinyl substituents derived from classical NHCs. The HOMO–LUMO energy gap of **1-E** (E = P: 4.15 eV; E = As: 3.86 eV)[18] is the narrowest among dipnictenes reported thus far.[12] Remarkably, unlike classical dipnictenes **II**, the HOMO of **IV** is mainly the E=E π bond, which is very high lying and enables the isolation of stable radical cations[20] (**IV**)$^{\cdot+}$ by 1e oxidation of **IV**. The electronic features of **IV** further prompted us to explore their suitability as ligands in transition-metal chemistry and to probe the synthetic viability of stable metalloradicals.

Herein, we report the synthesis of dipnictene complexes [(**1-E**)Fe(CO)$_3$] (**2-E**) and their sequential 1e oxidation to yield the corresponding stable radical cations [(**1-E**)Fe(CO)$_3$]$^{\cdot+}$ and dications [(**1-E**)Fe(CO)$_3$]$^{2+}$ (Schemes 1 and 2).
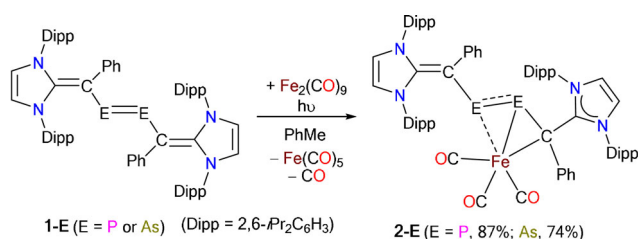
Scheme 1. Synthesis of Fe^0 complexes **2-P** and **2-As**.
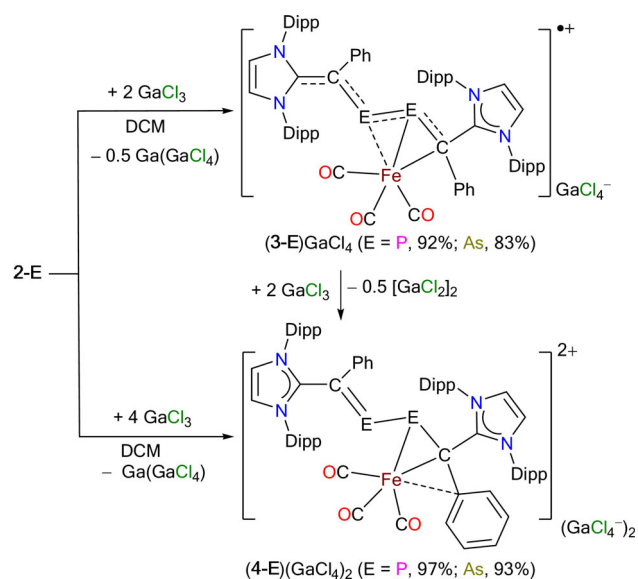
Scheme 2. Synthesis of (**3-E**)GaCl$_4$ and (**4-E**)(GaCl$_4$)$_2$ (E = P or As).

Results and Discussion

The Fe^0 complexes [(**1-E**)Fe(CO)$_3$] (**2-E**) were prepared by UV irradiation of a THF solution of the respective divinyldipnictene {(IPr)C(Ph)E}$_2$ (**1-E**) (E = P or As) and Fe$_2$(CO)$_9$ (Scheme 1). Complexes **2-E** are brown crystalline solids, soluble in common or-

ganic solvents (Et$_2$O, benzene, toluene, and THF), and are stable under an inert gas atmosphere. The ^{1}H NMR spectra of **2-E** exhibit well-resolved resonances for the (IPr)CPh moieties, which are fully consistent with the ^{13}C{^{1}H} NMR spectra (see the Supporting Information). The ^{31}P{^{1}H} NMR spectrum of **2-P** shows two doublets at −9.2 and −26.6 ppm ($^1J_{PP}$ = 363 Hz), indicating the presence of distinct coordination environments around the P atoms.

The solid-state molecular structures of **2-E** determined by X-ray diffraction studies (Figure 2) correlate well with the solution NMR data. The structures of **2-E** reveal a *trans*-bent geometry along the E=E bond, which binds to the Fe atom in a side-on fashion. The Fe atom in **2-E** is at the center of a distorted trigonal-bipyramidal geometry and features three terminal CO ligands. One of the vinylic carbon atoms of the (IPr)C(Ph) moieties binds to the Fe atom, whereas the second remains free. Thus, like anionic allylic ligands,[21] the neutral **1-E** molecule serves as a 4e donor in **2-E** (see below). The E–E bond lengths of **2-P** (2.145(6) Å) and **2-As** (2.354(6) Å) are longer than those of **1-P** (2.062(1) Å)[18b] and **1-As** (2.296(3) Å),[18a] respectively (Table 1). They are, however, still shorter than the calculated E—E single-bond lengths (2.20 Å, E = P; 2.46 Å, E = As).[22] The η^3-EEC$_{vinyl}$ coordination of **1-E** results in deplanarization of the C$_2$E$_2$C$_2$ scaffold in **2-E**, which has a dihedral angle of 8.63 (**2-P**) or 13.91° (**2-As**). Because of the transfer of π-electron density towards the Fe atom of the Lewis acidic Fe(CO)$_3$ unit, the C1—C2 bond lengths of **2-P** (1.496(5) Å) and **2-As** (1.459(1) Å) become longer and comparable to C–C single-bond lengths.[22] Interestingly, the C3–C4 bond lengths of **2-P** (1.375(7) Å) and **2-As** (1.385(1) Å) remain comparable to those of **1-P** (1.387(2) Å)[18b] and **1-As** (1.376(2) Å),[18a] respectively. As expected, the C4—E2 bond lengths (1.813(8) Å in **2-P** and 1.934(1) Å in **2-As**) are shorter than the C2—E1 bond lengths (1.842(6) Å in **2-P** and 1.959(9) Å in **2-As**). These bond lengths are longer than those in **1-P** (1.785(1) Å) and **1-As** (1.919(1) Å), and thus
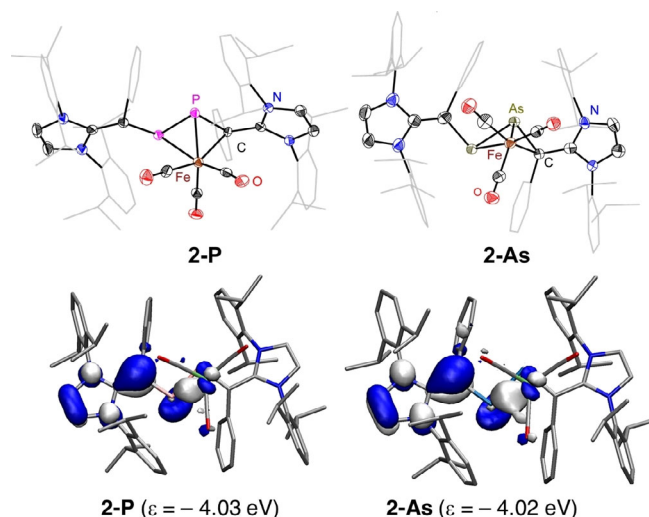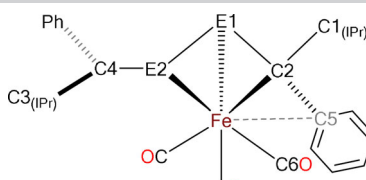

Figure 2. Solid-state molecular structures of **2-P** and **2-As** (top). H and minor disordered atoms have been omitted for clarity. HOMOs of **2-P** and **2-As** (bottom) calculated at the B3LYP+D3(BJ)/def2-TZVPP//B3LYP+D3(BJ)/def2-SVP level of theory (isovalue 0.06). H atoms have been omitted for clarity.

⤢⤢ These are not the final page numbers!

Table 1. Selected bond lengths [Å] and angles [°] of **1-E**, **2-E**, (**3-E**)GaCl$_4$, and (**4-E**)(GaCl$_4$)$_2$.

	C1–C2	C3–C4	C2–E1	C4–E2	E1–E2	Fe–C2	Fe–E1	Fe–E2/Fe–C5[b]	C2–E1–E2	E2–Fe–C6
1-P[a]	1.387(2)	–	1.785(1)	–	2.062(1)	–	–	–	102.6(1)	–
2-P	1.496(5)	1.375(7)	1.842(6)	1.813(8)	2.145(6)	2.162(6)	2.262(5)	2.475(5)	98.4(2)	163.4(5)
(**3-P**)$^{•+}$	1.470(7)	1.429(7)	1.826(5)	1.771(5)	2.197(2)	2.149(5)	2.240(2)	2.495(1)	91.4(2)	168.4(8)
(**4-P**)$^{2+}$	1.482(2)	1.470(3)	1.819(4)	1.700(7)	2.219(3)	2.084(2)	2.320(5)	2.190(2)	107.9(6)	–
1-As[a]	1.376(2)	–	1.919(1)	–	2.296(3)	–	–	–	98.99(4)	–
2-As	1.459(1)	1.385(1)	1.959(9)	1.934(1)	2.354(6)	2.169(1)	2.364(5)	2.567(5)	90.9(3)	167.4(1)
(**4-As**)$^{2+}$	1.476(3)	1.461(3)	1.957(3)	1.820(3)	2.454(4)	2.089(3)	2.423(5)	2.186(3)	105.9(7)	–

[a] Structures have a center of inversion. [b] The *ipso*-C$_{Ph}$–Fe interaction only in the dications (**4-E**)$^{2+}$.

indicate reduced π conjugation in **2-E**. The Fe–P1 (2.262(5) Å) bond in **2-P** is marginally longer than that of the η^1-diphosphene complex [(Mes*P)$_2$Fe(CO)$_4$] (2.215(1) Å) (Mes* = 2,4,6-tBu$_3$C$_6$H$_2$).[14g] The Fe–P2 (2.475(5) Å) bond is, however, longer than the sum of the Fe and P covalent radii, indicating a weak interaction. A similar trend is also visible for the Fe–As1 (2.364(5) Å) and Fe–As2 (2.567(5) Å) bond lengths of **2-As**. The Fe–C2 bond lengths of **2-P** (2.162(6) Å) and **2-As** (2.169(1) Å) are comparable to those found for π-allyl iron complexes (2.16 Å).[23]

The optimized geometries of **2-P** and **2-As** calculated at the B3LYP + D3(BJ)/def2-SVP level of theory (Figure S29, Tables S3 and S4 in the Supporting Information) are in good agreement with their solid-state molecular structures. The HOMOs of **2-P** and **2-As** are π-type orbitals (Figure 2) mainly located at the C$_{IPr}$=C$_{vinyl}$ (C3=C4) bond with some contributions from the same imidazole ring and iron d orbitals. The nature of the bonding interaction between Fe(CO)$_3$ and **1-E** fragments to form **2-E** was analyzed by energy decomposition analysis (EDA).[24] According to calculations, the bonding has approximately 10% dispersion, 42% electrostatic, and 47% orbital interactions. For **2-E**, EDA suggests donor–acceptor-type interactions between Fe(CO)$_3$ and **1-E** fragments (Figure 3a). The best fragmentation representation was selected by means of the orbital interaction energy term ΔE_{orb}, which indicates how much the orbitals relax on going from the fragments to the final state of a molecule. Thus, a small absolute value of ΔE_{orb} indicates that the selected electronic structure of the fragments matches with that of the real molecule. Consequently, the best electronic-structure representation is the one that leads to the smaller absolute value of ΔE_{orb} (see Table S17 in the Supporting Information). The singlet electronic state of Fe(CO)$_3$ has a fully occupied 3d$_{xz}$ orbital (e in C$_{3v}$ symmetry), and two empty 3d$_{yz}$ (e) and 4s (a$_1$) orbitals. The empty orbitals of Fe(CO)$_3$ interact with the symmetry-matching doubly occupied π orbitals (HOMO and HOMO−3) located at the central CE$_2$C moiety. The occupied orbital at Fe(CO)$_3$ interacts with the LUMO at the CE$_2$C unit.
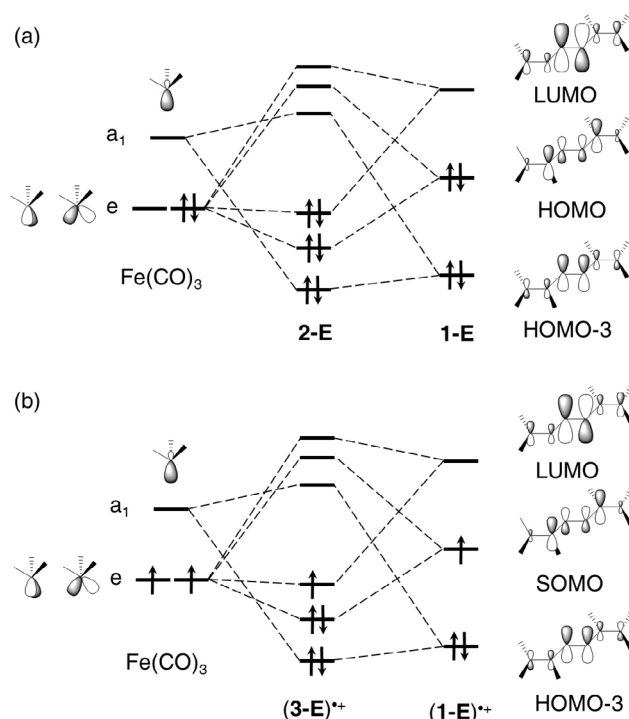

Figure 3. Qualitative molecular orbital diagrams showing the interactions between a) Fe(CO)$_3$ (C$_{3v}$ symmetry) and **1-E** (E = P and As) to form **2-E** (E = P and As) and b) Fe(CO)$_3$ (C$_{3v}$ symmetry) and (**1-E**)$^{•+}$ (E = P and As) to form (**3-E**)$^{•+}$ (E = P and As). For the sake of clarity, only the orbitals associated with bonding are considered.

The cyclic voltammograms (CVs) of **2-P** ($E_{1/2}$ = −0.85, +0.17 V) and **2-As** ($E_{1/2}$ = −0.82, +0.27 V) show two main redox events (Figure S1 in the Supporting Information), which may be assigned to the corresponding radical cations and dications, respectively. Indeed, addition of two equivalents of GaCl$_3$ to a red solution of **2-P** or **2-As** in CH$_2$Cl$_2$ immediately led to the formation of a violet solution.[25] After workup, the radical cations (**3-E**)GaCl$_4$ were isolated as violet solids (Scheme 2). Consistent with the CVs, further oxidation of (**3-**

These are not the final page numbers! ↗↗

E)GaCl$_4$ to the dicationic species (**4-E**)(GaCl$_4$)$_2$ is also viable with GaCl$_3$. (**4-E**)(GaCl$_4$)$_2$ are red crystalline solids, which can also be prepared directly by one-pot reactions of **2-E** with four equivalents of GaCl$_3$. Both (**3-E**)GaCl$_4$ and (**4-E**)(GaCl$_4$)$_2$ are stable in solution and in the solid-state under an inert gas atmosphere. The dications (**4-E**)(GaCl$_4$)$_2$ exhibit well-resolved ^{1}H and ^{13}C{^{1}H} NMR signals for the (IPr)CPh moieties. The ^{31}P{^{1}H} NMR spectrum of (**4-P**)(GaCl$_4$)$_2$ displays two doublets at $+0.03$ and $+454.9$ ppm ($^1J_{PP} = 352$ Hz), which are downfield-shifted compared to those of **2-P** (-9.2, -26.6 ppm). The signal at $+0.03$ ppm is comparable with those of phosphides,[26] whereas the signal at $+454.9$ ppm is consistent with those of phosphaalkenes.[27]

The molecular structures of (**3-P**)$^{•+}$, (**4-P**)$^{2+}$ (Figure 4), and (**4-As**)$^{2+}$ (Figure S28 in the Supporting Information) show *trans*-bent geometries along the E–E bond. The η^3-EEC$_{vinyl}$ coordination mode at the Fe atom remained virtually the same in **2-P** and (**3-P**)$^{•+}$, except for some alternations in the bond parameters (Table 1). Interestingly, the side-on η^3-EEC$_{vinyl}$ bonding to the Fe atom in (**4-P**)$^{2+}$ and (**4-As**)$^{2+}$ does not persist, and instead the Fe atom binds to only one of the E atoms in an end-on fashion and has a short Fe–*ipso*-C$_{Ph}$ contact. This leads to a new η^3-EC$_{vinyl}$C$_{Ph}$ coordination mode of the ligand at the Fe atom. Theoretical calculations (see below) support the preference of end-on η^3-EC$_{vinyl}$C$_{Ph}$-coordination in (**4-P**)$^{2+}$ over the side-on η^3-EEC$_{vinyl}$ coordination, as shown by **2-E** and (**3-P**)$^{•+}$. This type of redox-induced coordination shuttling is unprecedented in dipnictene chemistry. The P1–P2 bond length of (**3-P**)$^{•+}$ (2.197(2) Å) is longer than those of **2-P** (2.145(6) Å), **1-P** (2.062(1) Å),[18b] and (**1-P**)$^{•+}$ (2.106(7) Å)[20a] (Table 1), but matches well with the calculated P–P single-bond length (ca. 2.20 Å).[22] The C4–P2 (1.771(5) Å) and C2–P1 (1.826(5) Å) bond lengths of (**3-P**)$^{•+}$ are smaller than those of **2-P** (1.813(8) and 1.842(6) Å, respectively), but longer than that of (**1-P**)$^{•+}$ (1.744(2) Å).[20a] The C3–C4 bond length in (**3-P**)$^{•+}$ (1.429(7) Å) is larger than that of **2-P** (1.375(7) Å), while the C1–C2 bond length of (**3-P**)$^{•+}$ (1.470(7) Å) is marginally smaller than that of **2-P** (1.496(5) Å). The Fe1–P1 (2.240(2) Å) and Fe1–C2 (2.149(5) Å) bond lengths of (**3-P**)$^{•+}$ are shorter than those of **2-P**. The Fe1–P2 (2.495(1) Å) bond length is slightly longer than that of **2-P** (2.475(5) Å). The P1–P2 bond length of (**4-P**)$^{2+}$ (2.219(3) Å) is the longest among (**3-P**)$^{•+}$ (2.197(4) Å), **2-P** (2.145(6) Å), and (**1-P**)$^{2+}$ (2.192(1) Å) (Table 1). A similar trend in the As–As bond lengths can also be seen for (**4-As**)$^{2+}$ (2.454(4) Å), **2-As** (2.354(6) Å), and (**1-As**)$^{2+}$ (2.419(1) Å). In (**4-E**)$^{2+}$, the C4–P2 (1.700(7) Å) and C4–As2 (1.820(3) Å) bond lengths are smaller than those of C2–P1 (1.819(4) Å) and C2–As1 (1.957(3) Å), respectively. The former are consistent with the C=E double bond lengths of phosphaalkenes[28] and arsaalkenes,[29] while the latter are comparable to C–E (E = P or As) single-bond lengths.[22] Similarly, the Fe1–As1 (2.423(5) Å) and Fe1–C2 (2.089(3) Å) bond lengths of (**4-As**)$^{2+}$ are also shorter than those of **2-As**. The C1–C2 (1.482(2) Å) bond length of (**4-P**)$^{2+}$ is slightly longer than that of (**3-P**)$^{•+}$ (1.470(7) Å), but shorter with respect to that of **2-P** (1.496(5) Å).
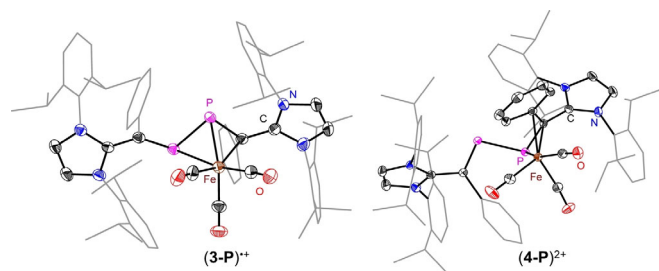
The optimized geometries (Figure S29 in the Supporting Information) at the B3LYP+D3(BJ)/def2-SVP level of theory are in good agreement with the X-ray diffraction (Table 1) structures of (**3-P**)$^{•+}$ and (**4-E**)$^{2+}$ (Tables S5–S8 in the Supporting Information). The elongation of the E–E bond length from **2-E** to (**3-E**)$^{•+}$ is in line with the slight lowering of the E–E bond order from **2-E** (E=P 1.09, As 1.04) to (**3-E**)$^{•+}$ (E=P 1.05, As 0.98) (Table S10 in the Supporting Information). The SOMO of (**3-E**)$^{•+}$ (Figure 5 a) is the C$_{IPr}$=C$_{vinyl}$ π bond with some contribution from the d orbital of the Fe(CO)$_3$ moiety. The LUMO of (**3-E**)$^{•+}$ is the other C$_{IPr}$–C$_{vinyl}$ π-bond close to the Fe atom with a discrete contribution of the p orbital of the E atom (Figures S32 and S33 in the Supporting Information). The localized Mulliken atomic spin density (Figure 5 b) for (**3-E**)$^{•+}$ reveals that the unpaired electron is mainly located at the iron atom (E=P, 0.62 e; As, 0.54 e). Notably, the spin density at the E atoms (0.02–0.08 e) is rather low compared to that at the vinylic carbon atom of (**3-E**)$^{•+}$ (E=P, 0.30 e; As, 0.36 e). We also performed a Local Spin Analysis, in which the expectation value of the spin-squared operator is decomposed into atomic (local spins) and diatomic terms.[30] The sum of the local spin atomic expectation values for Fe(CO)$_3$ (E=P, 0.379; As, 0.312) and C$_2$E$_2$ (E=P,
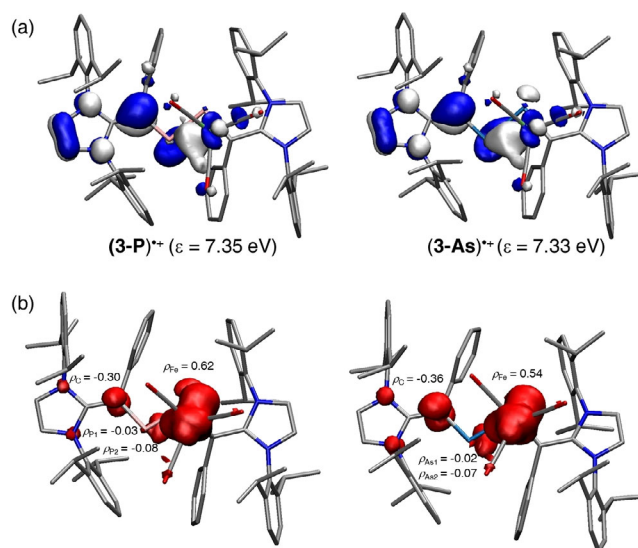

(a)

(**3-P**)$^{•+}$ ($\varepsilon = 7.35$ eV)   (**3-As**)$^{•+}$ ($\varepsilon = 7.33$ eV)

(b)

$\rho_C = -0.30$ $\rho_{Fe} = 0.62$ $\rho_C = -0.36$ $\rho_{Fe} = 0.54$
$\rho_{P1} = -0.03$ $\rho_{As1} = -0.02$
$\rho_{P2} = -0.08$ $\rho_{As2} = -0.07$

Figure 5. a) SOMOs of (**3-P**)$^{•+}$ and (**3-As**)$^{•+}$ at the B3LYP+D3(BJ)/def2-TZVPP//B3LYP+D3(BJ)/def2-SVP level of theory (isovalue 0.06). H atoms have been omitted for clarity. b) Spin density (isovalue 0.004 a.u.) and Mulliken spin-density plots of (**3-P**)$^{•+}$ and (**3-As**)$^{•+}$.

(**3-P**)$^{•+}$ (**4-P**)$^{2+}$

Figure 4. Solid-state molecular structures of (**3-P**)$^{•+}$ and (**4-P**)$^{2+}$. H atoms, solvent molecule(s), and GaCl$_4^-$ anion(s) have been omitted for clarity (see Table 1 for selected bond angles and lengths).

↖↖ These are not the final page numbers!

Chemistry–A European Journal

Full Paper
doi.org/10.1002/chem.202100213

Chemistry Europe
European Chemical
Societies Publishing

0.409, As, 0.467) suggest that the radical cations (**3-P**)$^{\bullet+}$ are stabilized by delocalization of the unpaired electron over the FeE$_2$C framework (Figure S37 in the Supporting Information). Strikingly, the oxidation of **2-E** to (**3-E**)$^{\bullet+}$ and of (**3-E**)$^{\bullet+}$ to (**4-E**)$^{2+}$ weakens the interaction between (**1-E**)$^{n+}$ ($n = 2$, 1, or 0) and Fe(CO)$_3$ moieties. Thus, the dissociation energies for the coordination of Fe(CO)$_3$ in (**4-E**)$^{2+}$ (E = P, 42.6; As, 42.4 kcal mol^{-1}) are lower than those of (**3-E**)$^{\bullet+}$ (E = P, 47.6; As, 51.5 kcal mol^{-1}), which are lower than those of **2-E** (E = P, 55.5; As, 59.8 kcal mol^{-1}) (Table S17 in the Supporting Information).

We also analyzed the nature of the bonding interactions by the EDA using different fragmentation schemes (see Figure S44 in the Supporting Information).[31] The coordination of Fe(CO)$_3$ to (**1-E**)$^{\bullet+}$ to form (**3-E**)$^{\bullet+}$ (Figure 3 b) occurs through the triplet reference state (e^{1}e^{1}a$_1^0$) of the iron moiety. The bonding nature in (**3-E**)$^{\bullet+}$ ($\approx 10\%$ dispersion, $\approx 47\%$ electrostatic, and $\approx 43\%$ orbital interactions) is similar to that of **2-E**, but the orbital interaction becomes weaker since back-donation involves only one electron from the Fe(CO)$_3$ to the LUMO of (**1-E**)$^{\bullet+}$. Thus, the coordination also becomes weaker ($\Delta E_{int} = -86.4$, E = P; $\Delta E_{int} = -88.6$ kcal mol^{-1}, E = As).

The X-band EPR spectrum of (**3-P**)GaCl$_4$ ($g_{iso} = 2.0959$) at 298 K exhibits a doublet of doublets due to coupling of the unpaired electron with two magnetically inequivalent ^{31}P ($I = 1/2$) nuclei (Figure 6). The X-band EPR spectrum of (**3-As**)GaCl$_4$ ($g_{iso} = 2.0539$) at 298 K shows a multiplet with poorly resolved hyperfine components due to coupling of the unpaired electron with two magnetically inequivalent ^{73}As ($I = 3/2$) nuclei (Figure 6). The magnitude of the hyperfine coupling constant (hfc) in (**3-P**)GaCl$_4$ ($A_{iso}(^{31}$P$) = 43$ MHz) is comparable to those of a diphosphene–Cr radical cation (45 MHz)[15] and carbene-stabilized radical cations (35–44 MHz).[32] The calculated hfc values at the B3LYP/def2-TZVPP level of theory show a strong contribution of the P1 (196.5 MHz) and As1 (145.8 MHz) nuclei directly attached to the iron atom (Table S11 in the Supporting Information).

In line with the experimental observation, calculations (Scheme S1 in the Supporting Information) support the preference of η^3-EC$_{vinyl}$C$_{Ph}$ bonding mode of the ligand in (**4-E**)$^{+2}$ over the η^3-EEC$_{vinyl}$ bonding style. The latter is preferred in (**3-E**)$^{\bullet+}$ and **2-E**. The isomeric model compounds [(**4-E**)$^{2+}$]$^{\#}$ featuring a similar η^3-EEC$_{vinyl}$ coordination mode were found to be energetically less stable by 7.1 kcal mol^{-1} (E = P) and 9.0 kcal mol^{-1} (E = As) than the isolated examples (**4-E**)(GaCl$_4$)$_2$ with the η^3-EC$_{vinyl}$C$_{Ph}$ bonding mode. The η^3-EEC$_{vinyl}$ to η^3-EC$_{vinyl}$C$_{Ph}$ coordination shuttling is unfavorable for **2-E** ($\Delta G = 37.5$ kcal mol^{-1}, E = P; 36.1 kcal mol^{-1}, E = As) and (**3-E**)$^{\bullet+}$ ($\Delta G = 19.4$ kcal mol^{-1}, E = P; 18.0 kcal mol^{-1}, E = As; Scheme S1 in the Supporting Information). The HOMO of (**4-E**)(GaCl$_4$)$_2$ (Figures S34 and S35 in the Supporting Information) is the σ-type orbital mainly located at the E–E bond. The HOMO−1 is located at the C$_{vinyl}$–Fe, E–E, and E–Fe bonds with a small contribution from the phenyl substituent. The LUMO is mainly the antibonding C$_{iPr}$= C$_{vinyl}$ bond with a significant contribution from a p-type orbital of one of the pnictogen atoms. The NPA atomic partial charges for (**4-E**)(GaCl$_4$)$_2$ (Table S10 in the Supporting Information) reveal a positive charge at the Fe(CO)$_3$ moiety of +0.35 e (E = P) and +0.33 e (E = As), indicating weaker donation from the ligand.

Further bonding insights were obtained by the EDA calculations. Donor–acceptor-type interactions represent the best bonding description. Compared to **2-E** and (**3-E**)GaCl$_4$, the interactions in (**4-E**)(GaCl$_4$)$_2$ become more orbital stabilized ($\approx 9\%$ dispersion, $\approx 37\%$ electrostatic, and $\approx 54\%$ orbital). In absolute values, the electrostatic interaction decreases by 38.0 kcal mol^{-1} for (**4-P**)(GaCl$_4$)$_2$ and 38.5 kcal mol^{-1} for (**4-E**)(GaCl$_4$)$_2$. The UV/Vis spectra of **2-P** ($\lambda_{max} = 373$ and 459 nm) and **2-As** ($\lambda_{max} = 354$ and 475 nm) exhibit two main absorptions (Figures S20 and S21 in the Supporting Information), which, on the basis of TD-DFT calculations, can be assigned to H−1/H→L and H→L+1 transitions, respectively (Tables S17 and S18 in the Supporting Information; H = HOMO and L = LUMO). The UV/Vis spectra of (**3-E**)GaCl$_4$ (Figures S22 and S23 in the Supporting Information) show two absorptions ($\lambda_{max} = 462$ and 508 nm, E = P; 458 and 510 nm, E = As) in the visible region, which are related to S(α)→L and H(β)→L transitions, respectively (Tables S19 and S20 in the Supporting Information).[33] The UV/Vis absorption band at 518 nm (E = P) or 530 nm (E = As) for (**4-E**)(GaCl$_4$)$_2$ (Figures S22 and S23 in the Supporting Information) is related to H→L/L+1 transitions (Tables S21 and S22 in the Supporting Information). The IR spectra of **2-P** (1876, 1909, 1972 cm^{-1}), (**3-P**)GaCl$_4$ (1933, 1954, 2013 cm^{-1}), and (**4-P**)(GaCl$_4$)$_2$ (2025, 2054, 2076 cm^{-1}) exhibit three bands for the CO stretching vibrations (Figures S14, S16, and S18 in the Supporting Information). A similar trend of increasing wavenumber can also be seen for the arsenic derivatives (Figures S15, S17, and S19 in the Supporting Information), which is consistent with depletion of the electron density at the iron atom on sequential 1e oxidation from **2-E** and (**3-E**)GaCl$_4$, resulting in weaker dπ$_{Fe}$→π*$_{CO}$ backbonding from **2-E** to (**3-E**)GaCl$_4$ to (**4-E**)(GaCl$_4$)$_2$.
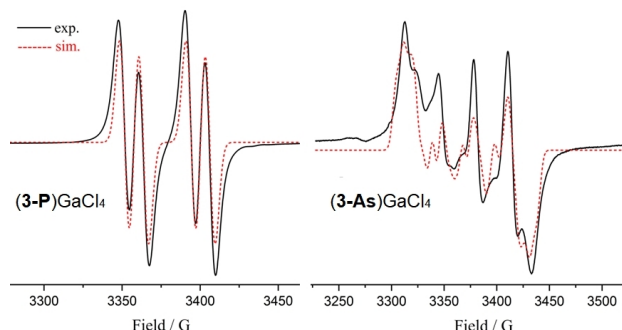

Figure 6. EPR spectra of (**3-P**)GaCl$_4$ and (**3-As**)GaCl$_4$ (in THF, 298 K). Simulation parameters: $g = 2.0960$, $A_{iso}(^{31}$P$)$ 311.9 MHz, $A_{iso}(^{31}$P$)$ 87.2 MHz, lw = 2.44 mT [(**3-P**)GaCl$_4$]; $g = 2.0539$, $A_{iso}(^{75}$As$)$ 424.6 MHz, $A_{iso}(^{75}$As$)$ 82.7 MHz, $A_{iso}(^{14}$N$)$ 126.1 MHz, $A_{iso}(^{14}$N$)$ 50.0 MHz, lw = 3.95 mT [(**3-As**)GaCl$_4$].

Conclusion

We have reported the synthesis, structure, and redox chemistry of two Fe^0 complexes **2-E** (E = P or As) featuring unconventional divinyldipnictene ligands as crystalline solids. The sequential 1e oxidation of **2-E** with GaCl$_3$ was shown to afford crystalline

Chemistry–A European Journal

Full Paper
doi.org/10.1002/chem.202100213

Chemistry Europe
European Chemical
Societies Publishing

metalloradical cations (**3-E**)GaCl$_4$ and dications (**4-E**)(GaCl$_4$)$_2$. The formation of the latter occurs with unprecedented η^3-EEC$_{vinyl}$- to η^3-EC$_{vinyl}$C$_{Ph}$-coordination shuttling, which has been rationalized by theoretical calculations. Compounds (**3-E**)GaCl$_4$ were characterized by cyclic voltammetry, EPR spectroscopy, UV/Vis spectroscopy, and single-crystal X-ray diffraction. The studies revealed that (**3-E**)GaCl$_4$ are stabilized by delocalization of the unpaired electron over the CE$_2$Fe moiety, while the spin density is mainly located at the Fe and vinylic carbon atoms. The findings are expected to attract further interest in the isolation and exploration of other metalloradicals based on **1-E**.

Experimental Section

Deposition Numbers 1939894, 1998503, 1998504, 1998505, and 1998506 contain the supplementary crystallographic data for this paper. These data are provided free of charge by the joint Cambridge Crystallographic Data Centre and Fachinformationszentrum Karlsruhe Access Structures service www.ccdc.cam.ac.uk/structures.

Conflict of interest

The authors declare no conflict of interest.

[1] a) K. Kato, A. Osuka, *Angew. Chem. Int. Ed.* **2019**, *58*, 8978–8986; *Angew. Chem.* **2019**, *131*, 9074–9082; b) S. Kundu, S. Sinhababu, V. Chandrasekhar, H. W. Roesky, *Chem. Sci.* **2019**, *10*, 4727–4741; c) R. S. Ghadwal, *Synlett* **2019**, *30*, 1765–1775; d) G. W. Tan, X. P. Wang, *Chin. J. Chem.* **2018**, *36*, 573–586; e) K. Chandra Mondal, S. Roy, H. W. Roesky, *Chem. Soc. Rev.* **2016**, *45*, 1080–1111; f) C. D. Martin, M. Soleilhavoup, G. Bertrand, *Chem. Sci.* **2013**, *4*, 3020–3030; g) T. Chivers, J. Konu, *Comprehensive Inorganic Chemistry II: From Elements to Applications, Vol. I* (Eds.: J. Reedijk, K. Poeppelmeier), Elsevier, Amsterdam, **2013**, pp. 349–373; h) S. González-Gallardo, F. Breher, *Comprehensive Inorganic Chemistry II*, 2nd ed. (Eds.: J. Reedijk, K. Poeppelmeier), Elsevier, Amsterdam, **2013**, pp. 413–455; i) J. Kanu, T. Chivers, *Stable Radicals: Fundamentals and Applied Aspects of Odd-Electron Compounds*, 1st ed. (Ed.: R. G. Hicks), Wiley, Chichester, **2010**, pp. 381–406; j) M. K. Sharma, F. Ebeler, T. Glodde, B. Neumann, H.-G. Stammler, R. S. Ghadwal, *J. Am. Chem. Soc.* **2021**, *143*, 121–125; k) M. K. Sharma, D. Rottschäfer, T. Glodde, B. Neumann, H.-G. Stammler, R. S. Ghadwal, *Angew. Chem. Int. Ed.* **2021**, *60*, https://doi.org/10.1002/anie.202017078.

[2] a) A. Studer, D. P. Curran, *Angew. Chem. Int. Ed.* **2016**, *55*, 58–102; b) Q. Cao, L. M. Dornan, L. Rogan, N. L. Hughes, M. J. Muldoon, *Chem. Commun.* **2014**, *50*, 4524–4543; c) T. D. Beeson, A. Mastracchio, J.-B. Hong, K. Ashton, D. W. C. MacMillan, *Science* **2007**, *316*, 582–585.

[3] a) T. Ullrich, P. Pinter, J. Messelberger, P. Haines, R. Kaur, M. M. Hansmann, D. Munz, D. M. Guldi, *Angew. Chem. Int. Ed.* **2020**, *59*, 7906–7914; b) X. Ai, Y. Chen, Y. Feng, F. Li, *Angew. Chem. Int. Ed.* **2018**, *57*, 2869–2873; c) X. Hu, W. Wang, D. Wang, Y. Zheng, *J. Mater. Chem. C*

2018, *6*, 11232–11242; d) Y. Huang, E. Egap, *Polym. J.* **2018**, *50*, 603–614; e) D. A. Wilcox, V. Agarkar, S. Mukherjee, B. W. Boudouris, *Annu. Rev. Chem. Biomol. Eng.* **2018**, *9*, 83–103; f) Y. Wang, M. Frasconi, J. F. Stoddart, *ACS Cent. Sci.* **2017**, *3*, 927–935.

[4] a) C.-Y. Lin, P. P. Power, *Chem. Soc. Rev.* **2017**, *46*, 5347–5399; b) M. M. Schwab, D. Himmel, S. Kacprzak, D. Kratzert, V. Radtke, P. Weis, K. Ray, E. W. Scheidt, W. Scherer, B. de Bruin, S. Weber, I. Krossing, *Angew. Chem. Int. Ed.* **2015**, *54*, 14706–14709.

[5] a) N. P. van Leest, R. F. J. Epping, K. M. van Vliet, M. Lankelma, E. J. van den Heuvel, N. Heijtbrink, R. Broersen, B. de Bruin, *Adv. Organomet. Chem., Vol. 70* (Eds.: P. J. Pérez, F. G. A. Stone, R. West), Academic Press, Cambridge, **2018**, pp. 71–180; b) E. Peris, R. H. Crabtree, *Chem. Soc. Rev.* **2018**, *47*, 1959–1968; c) T. Kégl, G. C. Fortman, M. Temprado, C. D. Hoff, *Physical Inorganic Chemistry* (Ed.: A. Bakac), Wiley, Hoboken, **2010**, pp. 429–494.

[6] a) R. Poli, *Chem. Rev.* **1996**, *96*, 2135–2204; b) W. I. Dzik, B. de Bruin, *Organometallic Chemistry, Vol, 37*, The Royal Society of Chemistry, Cambridge, **2011**, pp. 46–78; c) D. B. Leznoff, C. E. Hayes, G. Mund, *Encyclopedia of Inorganic and Bioinorganic Chemistry* (Ed.: R. A. Scott), Wiley, Hoboken, **2012**; d) X. Zheng, X. Wang, Z. Zhang, Y. Sui, X. Wang, P. P. Power, *Angew. Chem. Int. Ed.* **2015**, *54*, 9084–9087; e) J. C. Ott, H. Wadepohl, L. H. Gade, *Angew. Chem. Int. Ed.* **2020**, *59*, 9448–9452.

[7] a) U. Jahn, *Top. Curr. Chem.* **2011**, *320*, 323–451; b) U. Jahn, *Top. Curr. Chem.* **2011**, *320*, 191–322; c) U. Jahn, *Top. Curr. Chem.* **2011**, *320*, 121–189; d) D. Leifert, A. Studer, *Angew. Chem. Int. Ed.* **2020**, *59*, 74–108; e) B. Su, Z.-C. Cao, Z.-J. Shi, *Acc. Chem. Res.* **2015**, *48*, 886–896.

[8] a) Y. Hu, K. Lang, C. Li, J. B. Gill, I. Kim, H. Lu, K. B. Fields, M. Marshall, Q. Cheng, X. Cui, L. Wojtas, X. P. Zhang, *J. Am. Chem. Soc.* **2019**, *141*, 18160–18169; b) K. Lang, S. Torker, L. Wojtas, X. P. Zhang, *J. Am. Chem. Soc.* **2019**, *141*, 12388–12396; c) Y. Hu, K. Lang, J. Tao, M. K. Marshall, Q. Cheng, X. Cui, L. Wojtas, X. P. Zhang, *Angew. Chem. Int. Ed.* **2019**, *58*, 2670–2674; d) D. Shimizu, A. Osuka, *Chem. Sci.* **2018**, *9*, 1408–1423; e) W. Yang, H. Zhang, L. Li, C. M. Tam, S. Feng, K. L. Wong, W. Y. Lai, S. H. Ng, C. Chen, K. S. Chan, *Organometallics* **2016**, *35*, 3295–3300; f) C. Yoo, Y. Lee, *Angew. Chem. Int. Ed.* **2017**, *56*, 9502–9506.

[9] a) B. de Bruin, D. H. G. Hetterscheid, A. J. J. Koekkoek, H. Grützmacher, *Prog. Inorg. Chem.* **2007**, *55*, 247; b) R. Poli, *Angew. Chem. Int. Ed.* **2011**, *50*, 43–45; c) Y. Nakajima, Y. Nakao, S. Sakaki, Y. Tamada, T. Ono, F. Ozawa, *J. Am. Chem. Soc.* **2010**, *132*, 9934–9936.

[10] B. Twamley, C. D. Sofield, M. M. Olmstead, P. P. Power, *J. Am. Chem. Soc.* **1999**, *121*, 3357–3367.

[11] R. C. Fischer, P. P. Power, *Chem. Rev.* **2010**, *110*, 3877–3923.

[12] L. L. Liu, L. L. Cao, J. Zhou, D. W. Stephan, *Angew. Chem. Int. Ed.* **2019**, *58*, 273–277.

[13] M. Yoshifuji, *Eur. J. Inorg. Chem.* **2016**, 607–615.

[14] a) L. Weber, *Chem. Rev.* **1992**, *92*, 1839–1906; b) A. M. Caminade, J. P. Majoral, R. Mathieu, *Chem. Rev.* **1991**, *91*, 575–612; c) S. Gómez-Ruiz, E. Hey-Hawkins, *Coord. Chem. Rev.* **2011**, *255*, 1360–1386; d) S. Gómez-Ruiz, S. Zahn, B. Kirchner, W. Böhlmann, E. Hey-Hawkins, *Chem. Eur. J.* **2008**, *14*, 8980–8985; e) S. Gómez-Ruiz, E. Hey-Hawkins, *Dalton Trans.* **2007**, 5678–5683; f) A. H. Cowley, J. E. Kilduff, J. G. Lasch, N. C. Norman, M. Pakulski, F. Ando, T. C. Wright, *Organometallics* **1984**, *3*, 1044–1050; g) A. H. Cowley, J. E. Kilduff, J. G. Lasch, N. C. Norman, M. Pakulski, F. Ando, T. C. Wright, *J. Am. Chem. Soc.* **1983**, *105*, 7751–7752; h) S. Attali, F. Dahan, R. Mathieu, A. M. Caminade, J. P. Majoral, *J. Am. Chem. Soc.* **1988**, *110*, 1990–1991; i) K. M. Flynn, H. Hope, B. D. Murray, M. M. Olmstead, P. P. Power, *J. Am. Chem. Soc.* **1983**, *105*, 7750–7751; j) K. M. Flynn, M. M. Olmstead, P. P. Power, *J. Am. Chem. Soc.* **1983**, *105*, 2085–2086.

[15] W. Wang, C. Q. Xu, Y. Fang, Y. Zhao, J. Li, X. Wang, *Angew. Chem. Int. Ed.* **2018**, *57*, 9419–9424.

[16] S.-S. Asami, S. Ishida, T. Iwamoto, K. Suzuki, M. Yamashita, *Angew. Chem. Int. Ed.* **2017**, *56*, 1658–1662.

[17] B. Milián-Medina, J. Gierschner, *WIREs Comput. Mol. Sci.* **2012**, *2*, 513–524.

[18] a) M. K. Sharma, S. Blomeyer, B. Neumann, H. G. Stammler, R. S. Ghadwal, *Chem. Eur. J.* **2019**, *25*, 8249–8253; b) D. Rottschäfer, M. K. Sharma, B. Neumann, H.-G. Stammler, D. M. Andrada, R. S. Ghadwal, *Chem. Eur. J.* **2019**, *25*, 8127–8134.

[19] a) D. Rottschäfer, B. Neumann, H. G. Stammler, D. M. Andrada, R. S. Ghadwal, *J. Org. Chem.* **2020**, *85*, 14351–14359; b) M. K. Sharma, B.

↖↖ These are not the final page numbers!

Neumann, H.-G. Stammler, D. M. Andrada, R. S. Ghadwal, *Chem. Commun.* **2019**, *55*, 14669–14672.

[20] a) M. K. Sharma, D. Rottschäfer, S. Blomeyer, B. Neumann, H.-G. Stammler, M. van Gastel, A. Hinz, R. S. Ghadwal, *Chem. Commun.* **2019**, *55*, 10408–10411; b) M. K. Sharma, S. Blomeyer, B. Neumann, H.-G. Stammler, M. van Gastel, A. Hinz, R. S. Ghadwal, *Angew. Chem. Int. Ed.* **2019**, *58*, 17599–17603.

[21] Y. Heider, P. Willmes, D. Mühlhausen, L. Klemmer, M. Zimmer, V. Huch, D. Scheschkewitz, *Angew. Chem. Int. Ed.* **2019**, *58*, 1939–1944.

[22] a) P. Pyykkö, M. Atsumi, *Chem. Eur. J.* **2009**, *15*, 12770–12779; b) P. Pyykkö, M. Atsumi, *Chem. Eur. J.* **2009**, *15*, 186–197.

[23] U. Eberhardt, G. Mattern, *Chem. Ber.* **1988**, *121*, 1531–1534.

[24] Further details of EDA calculations are given in the Supporting Information.

[25] Two molecules of $GaCl_3$ are required for one-electron oxidation of **2-E** according to $2\,GaCl_3 \rightarrow (GaCl_4)^- + (GaCl_2)^+$. One-electron reduction of $(GaCl_2)^+$ gives $GaCl_2$, which undergoes disproportionation to form the stable mixed-valent Ga^I/Ga^{III} species $[Ga(GaCl_4)]$. The weakly coordinating anion $GaCl_4$ balances the charge of the oxidized radical cation species. See ref. [20a] for further details.

[26] a) N. Burford, C. A. Dyker, A. Decken, *Angew. Chem. Int. Ed.* **2005**, *44*, 2364–2367; b) C. L. Boulangé, *Encyclopedia of Analytical Science*, 3rd ed.

[Eds.: P. Worsfold, C. Poole, A. Townshend, M. Miró), Academic Press, Oxford, **2019**, pp. 319–327; c) O. Kühl, *Phosphorus-31 NMR Spectroscopy*, Springe, Heidelberg, **2009**.

[27] a) P. L. Floch, *Coord. Chem. Rev.* **2006**, *250*, 627–681; b) L. Weber, *Coord. Chem. Rev.* **2005**, *249*, 741–763; c) L. Weber, *Eur. J. Inorg. Chem.* **2000**, 2425–2441.

[28] F. Mathey, *Angew. Chem. Int. Ed.* **2003**, *42*, 1578–1604.

[29] a) M. Bouslikhane, H. Gornitzka, H. Ranaivonjatovo, J. Escudié, *Organometallics* **2002**, *21*, 1531–1533; b) D. Ghereg, N. Saffon, J. Escudié, K. Miqueu, J.-M. Sotiropoulos, *J. Am. Chem. Soc.* **2011**, *133*, 2366–2369.

[30] E. Ramos-Cordoba, E. Matito, I. Mayer, P. Salvador, *J. Chem. Theory Comput.* **2012**, *8*, 1270–1279.

[31] Considering the possibility of the $Fe(CO)_3$ moiety as a one-electron-less fragment for EDA leads to high orbital-energy terms.

[32] O. Back, B. Donnadieu, P. Parameswaran, G. Frenking, G. Bertrand, *Nat. Chem.* **2010**, *2*, 369–373.

[33] The α and β states are differentiated for the open-shell systems.

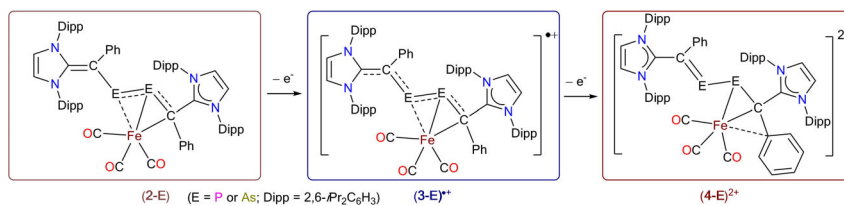# FULL PAPER

M. K. Sharma, D. Rottschäfer,
B. Neumann, H.-G. Stammler, S. Danés,
D. M. Andrada,* M. van Gastel, A. Hinz,
R. S. Ghadwal*

■■ – ■■

Metalloradical Cations and Dications Based on Divinyldiphosphene and Divinyldiarsene Ligands

(2-E)   (E = P or As; Dipp = 2,6-iPr$_2$C$_6$H$_3$)   (3-E)$^{•+}$ (4-E)$^{2+}$

Dipnictene-based metalloradicals: The metalloradicals (**3-E**)$^{•+}$ (E = P or As) are accessible as crystalline violet solids by 1e oxidation of divinyldipnictene Fe^0 complexes **2E**. Further 1e oxidation of (**3-E**)$^{•+}$ leads to unprecedented η^3-EEC$_{vinyl}$ to η^3-EC$_{vinyl}$C$_{Ph}$ coordination shuttling resulting in the dications (**4-E**)$^{2+}$.